Available online at www.sciencedirect.com
ScienceDirect
Atmospheric Environment 41 (2007) 9435–9451
ATMOSPHERIC ENVIRONMENT
www.elsevier.com/locate/atmosenv

Classification of multiple types of organic carbon composition in atmospheric particles by scanning transmission X-ray microscopy analysis

S. Takahama[a], S. Gilardoni[a], L.M. Russell[a,*], A.L.D. Kilcoyne[b]

[a]*Scripps Institution of Oceanography, University of California San Diego, 9500 Gilman Dr., Department 0221, La Jolla, CA 92093, USA*
[b]*Advanced Light Source, Lawrence Berkeley National Laboratory, Berkeley, CA 94720, USA*

Received 16 May 2007; received in revised form 1 August 2007; accepted 29 August 2007

Abstract

A scanning transmission X-ray microscope at the Lawrence Berkeley National Laboratory is used to measure organic functional group abundance and morphology of atmospheric aerosols. We present a summary of spectra, sizes, and shapes observed in 595 particles that were collected and analyzed between 2000 and 2006. These particles ranged between 0.1 and 12 μm and represent aerosols found in a large range of geographical areas, altitudes, and times. They include samples from seven different field campaigns: PELTI, ACE-ASIA, DYCOMS II, Princeton, MILAGRO (urban), MILAGRO (C-130), and INTEX-B. At least 14 different classes of organic particles show different types of spectroscopic signatures. Different particle types are found within the same region while the same particle types are also found in different geographical domains. Particles chemically resembling black carbon, humic-like aerosols, pine ultisol, and secondary or processed aerosol have been identified from functional group abundance and comparison of spectra with those published in the literature.

Keywords: Aerosol; Microscopy; Carbonaceous aerosol; Organic; Functional group; NEXAFS; XANES; STXM

1. Introduction

Atmospheric particles comprise sulfate, ammonium, nitrate, elemental carbon, organic compounds, trace metals, crustal elements, and water (Seinfeld and Pandis, 2006); organic material can account for 30–90% of the particle mass (Lim and Turpin, 2002) and yet the relevant properties of the organic fraction are not well characterized (Kanakidou et al., 2005; Fuzzi et al., 2006). To address this knowledge gap, mass spectrometry, spectroscopy, and chromatography techniques are often employed to measure bulk and single-particle chemical properties of ambient organic aerosols.

Hamilton et al. (2004) identified 10,000 chemical compounds in organic aerosol sampled in an urban environment using direct thermal desorption coupled to comprehensive gas chromatography-time-of-flight mass spectrometry (GCXGC-TOF/MS). This quantity of information is difficult to use for interpretation of atmospheric measurements and intractable for regional and global modeling.

*Corresponding author. Tel.: +1 858 534 4852; fax: +1 858 534 4851.
E-mail address: lmrussell@ucsd.edu (L.M. Russell).

1352-2310/$ - see front matter © 2007 Elsevier Ltd. All rights reserved.
doi:10.1016/j.atmosenv.2007.08.051

Data clustering and classification provides a means by which we can lump molecules or types of particles into characteristically similar groups, reducing the complexity of subsequent analyses. Zhang et al. (2005a) developed a sequential multivariate regression method for application to aerodyne aerosol mass spectrometer (AMS)-measured mass fragments of the size-resolved bulk organic fraction of particles to derive the contributions from two types: hydrocarbon-like and oxygenated organic aerosols (HOA and OOA, respectively). This technique has been applied to the analysis of field measurements in urban areas to show that these two types of compounds constitute most of the organic aerosol (Zhang et al., 2005b; Kondo et al., 2007). Single-particle mass spectrometry techniques have been able to use different clustering algorithms to provide information about the size and mixing states of inorganic and organic components of aerosols based on elemental and molecular fragment composition (Rhoads et al., 2003; Phares et al., 2003; Tolocka et al., 2005; Bein et al., 2005), but often the mass fragments of carbon-containing aerosols remain unresolved.

Particle morphology is also necessary for a complete understanding of how these organic compounds affect the way they acquire mass from the gas phase or interact with solar radiation (Kanakidou et al., 2005). For instance, shape affects surface area for reactions that control rates of photochemical aging (van Poppel et al., 2005) and direct radiative forcing by which particles scatter and absorb sunlight. Heterogeneities can affect predictions of many atmospheric processes, including bulk chemical kinetics, surface reactions, mass transport, thermodynamic partitioning, and phase transitions (Seinfeld and Pandis, 2006).

For investigation of single-particle morphology and composition, particle imaging techniques such as transmission electron microscopy (TEM), environmental scanning transmission electron microscopy (ETEM), scanning electron microscopy (SEM), and environmental scanning electron microscopy (ESEM) coupled with electron energy-loss spectroscopy (EELS) or energy-dispersive X-ray spectrometry (EDX) can correlate shape and chemistry (e.g., Hand et al., 2005; Johnson et al., 2005; Laskin et al., 2005, 2006), and additional properties such as hygroscopicity (Semeniuk et al., 2007). These electron microscopy techniques provide high spatial resolution, but the complementary spectroscopy methods provide limited information on chemical composition or risk inducing radiation damage in the sample (Warwick et al., 1997; Braun et al., 2005a).

Fuzzi et al. (2006) suggest possible organic aerosol classification categories based on source, and techniques by which the organic aerosol fraction can be used to map measurements to the suggested source categories. Near edge X-ray absorption fine structure (NEXAFS) spectrometry uses synchrotron-generated soft X-ray beams which provide the energy resolution necessary to distinguish organic functional groups absorbing at different bonding energies of carbon-containing molecules (e.g., Stöhr, 1992; Russell et al., 2002; Myneni, 2002; Maria et al., 2004; Braun, 2005). Samples are analyzed under atmospheric pressure, resulting in reduced loss of semi-volatile material commonly found in organic constituents of aerosols. We use this spectrometry method with a scanning transmission X-ray microscope (STXM) for analysis of our samples.

In microscopy analysis, discretion is warranted in using size and shape information for data clustering and also for general interpretation of the results, as spherical particles can be elongated or smeared against the substrate (Barkay et al., 2005), and loosely bound constituents of a particle may be disaggregated in the process of sample collection via impaction. Therefore, chemical properties are considered as the primary means of classification in this work.

Russell et al. (2002) and Maria et al. (2004) reported STXM analysis of particles collected from several different regions representing different types of aerosols: Eastern US combustion aerosol from Princeton, NJ, African mineral dust over the Caribbean Sea (PELTI campaign), Asian combustion aerosol over the Sea of Japan (ACE-ASIA campaign). In this study, we combine these particles with a meta-analysis of additional particles collected during DYCOMS II, MILAGRO, and INTEX B, providing several categories for chemical properties and morphologies observed in ambient particles, thereby relating them to the location and period during which they were collected.

2. Methods

2.1. Geospatial domain

Samples analyzed in this paper were collected during the Passing Efficiency Low Turbulence Inlet

(PELTI) experiment, a campaign to characterize aerosol in the Caribbean (Huebert et al., 2004); Aerosol Characterization Experiment (ACE-Asia), a campaign to study aerosol in China, Japan, and Korea (Huebert et al., 2003) during April 2001; Second Dynamics and Chemistry of Marine Stratocumulus field study (DYCOMS II), a study of marine stratocumulous clouds conducted during July 2001 southwest of San Diego, CA, USA (Stevens et al., 2003); Megacity Initiative: Local and Global Research Observations (MILAGRO), a mega-city characterization campaign involving measurement at an urban site (MCMA) and aloft via aircraft (MIRAGE C-130) during March 2006 (http://www.eol.ucar.edu/projects/milagro/); and INTEX-B, a campaign to measure Asian pollution outflow along the Pacific Northwest coast of the US in May 2006 (http://www.espo.nasa.gov/intex-b/). Samples collected at a ground site in Princeton, NJ, USA, in August 2003 (Maria et al., 2004) are also included in this analysis.

2.2. Sample collection and analysis

Particles were collected on silicon nitride windows (Si_3N_4; Silson Ltd.) mounted on a rotating impactor (Streaker; PIXE International, Inc.) for all samples except those samples in Princeton, NJ. For these samples, lacey-carbon TEM grids were used as the substrate. For both aircraft and ground site measurements, aluminum or copper tubing was used to draw air into the impactor at 1 Lpm. Sampled grids and windows were analyzed at the Advanced Light Source at Lawrence Berkeley National Laboratories (Berkeley, CA) Beamlines 5.3.2, 7.0.1, and 11.0.2 in a He-filled chamber maintained at 1 atm. Transmission of photons at energy levels between 278 and 305 eV was measured over a minimum spatial resolution of 30 nm and converted to optical density, using a protocol described by Russell et al. (2002) and Maria et al. (2004).

2.3. Spectral classification and analysis

Spectra were classified according to the presence of functional groups identified by Russell et al. (2002). Alkyl, ketonic carbonyl, carboxylic carbonyl, and alkene (or aromatic) groups are abbreviated as $R(CH_n)R'$, $R(C{=}O)R$, $R(C{=}O)OH$ and $R(C{=}C)R'$, respectively. R represents any alkyl chain, R′ represents H or any alkyl chain, and $n = 0$, 1, or 2 (Russell et al., 2002). π^*-bonds for molecules containing these functional groups absorb near 285 ± 0.2 eV ($R(C{=}C)R'$), 286.7 ± 0.2 ($R(C{=}O)R$), 287.7 ± 0.7 ($R(CH_n)R'$), and 288.7 ± 0.3 eV ($R(C{=}O)OH$). Additionally, carbonate (CO_3^{2-}) absorbs around 290.4 ± 0.2 eV and potassium (K) $L_{2,3}$ edges at 297.4 ± 0.2 and 299.9 ± 0.2 eV (Russell et al., 2002; Yoon et al., 2006). Images were aligned using the Zimba subroutine implemented in aXis2000 (http://unicorn.mcmaster.ca/aXis2000.html); energy levels were aligned a posteriori to account for shifts in spectra energies. Spectra were adjusted for background absorbance ($278 < eV < 283$) and normalized to total carbon content ($301 < eV < 305$) (Maria et al., 2004).

Spectra were classified using their full dimensionality (i.e. absorbance at energy levels scanned and interpolated over a grid consisting of 82 points between 280 and 305 eV), which can be more selective than classification based on pre-selected peak abundance. First, *k*-means and hierarchical clustering algorithms were applied on a data set after having removed 5% of the most extreme spectra as determined by Euclidean distance from the grand spectra average (thus reducing the possibility of creating classes that contain single samples). After application of these algorithms, group centers were used as a training set for *k*-nn to assign memberships for all spectra. Unsupervised classification algorithms excel at single-objective optimization, i.e. finding a solution which minimizes the sum-of-squares between spectra and cluster centers for all spectra. However, we qualitatively considered additional criteria for classification, such as our understanding of chemical similarity as determined by interpretation of the spectra, sampling conditions, times, and locations, and this information was incorporated through manual redistribution of spectra grouped by the quantitative algorithms. The final procedure increases the overall sum and variance of sum-of-squares from cluster centers, but effectively allows construction of a few groups with small within-cluster sum-of-square values that are believed to have atmospherically relevant similarities.

For semi-quantitative characterization of particle classes, deconvolution of the spectra was performed according to a method similar to that described by Lehmann et al. (2005) and Hopkins et al. (2007). Gaussian peaks with FWHM constrained to 0.5–2 eV were fitted at each of the peak locations described above and also at 289.7 eV, and two

broader peaks to represent σ^*-transitions at 294 and 303 eV constrained to 0.5–6 and 0.5–8 eV, respectively. The ionization threshold was approximated with an arctangent function with 1 eV FWHM.

For classes of spectra believed to contain black carbon, $\%sp^2$ hybridization was calculated (Hopkins et al., 2007) to characterize the graphitic nature of the particle. This value is calculated according to the equation

$$\%sp^2 = \left(\frac{A^{(sample)}_{R(C=C)R'}}{A^{(sample)}_{Total}} \times \frac{A^{(HOPG)}_{Total}}{A^{(HOPG)}_{R(C=C)R'}} \right) \cdot 100\%.$$

While Hopkins et al. (2007) used energies between 280 and 320 eV to calculate A_{Total}, we use energies between 280 and 305 because of data availability. Because the energy range used in normalization is consistent for both the samples and the reference HOPG spectra, the difference between our reported results and those of (Hopkins et al., 2007) is expected to be small.

2.4. Morphology classification

Particles can be found in many different types of shapes: single sphere, single irregular solid (e.g., crystal), and aggregate of many particles. For this analysis, the particles were classified visually as spherical or irregular based on the 285 eV STXM image of their impacted shape. Geometric sizes were calculated by averaging physical measurements along perpendicular axes of the particle. Heterogeneities can include agglomerations of a single phase of different chemical compositions or coexistence of multiple phases, which can occur in many different configurations (Seinfeld and Pandis, 2006). Although an exhaustive analysis of heterogeneities is beyond the scope of this work, a separate spectrum was assigned to each region of a single particle if the variation in spectra was significant.

2.5. Backtrajectory analysis

The National Oceanic and Atmospheric Administration Hybrid Single-Particle Lagrangian Integrated Trajectory (HYSPLIT, Draxler and Rolph, 2003; Rolph, 2003) model was used to calculate backtrajectories for a few scenarios. For these calculations, the FNL meteorological data were used as inputs. Following the recommendations of Gebhart et al. (2005), the trajectories were run in an ensemble mode to allow the model to effectively simulate over a range of initial starting locations and heights. A horizontal grid offset of 0.3 and a vertical offset of 0.1 sigma coordinates were specified for the simulation. According to the resolution of the FNL input data set, this corresponds to approximately 30 km horizontal and 90–120 m vertical displacement over 27 simulations for each ensemble.

2.6. Simultaneous filter measurements

During all field sampling campaigns in which samples for STXM analysis were collected, particles were concurrently collected on a collocated Teflon-filter sampler. These filters were analyzed by FTIR for organic functional groups (Maria et al., 2003, 2004). Some of these filters were analyzed by X-ray fluorescence (XRF) by Chester LabNet (Tigard, OG) for elemental composition to aid in source identification.

3. Results and discussion

Table 1 summarizes the particles included in our classification scheme. A total of 595 particles collected between 2000 and 2006 were analyzed. Altitudes of samples ranged between 30 and 4400 m. Of these particles, 244 were classified as being spherical; 54 contained heterogeneities. More than one spectrum may be associated with a single particle if its chemical heterogeneities are resolvable; this resulted in 680 different spectra. One-hundred and forty-two of these spectra were not interpretable either because the signal was either saturated or lost in the noise. The geometric diameters of particles analyzed spanned from 0.1 to 12 μm, with 364 particles below 1 μm. Over 80% of the 595 particles exhibited statistically significant spectral intensities below 283 eV, indicating that the majority of these organic particles were internally mixed with non-carbonaceous material (Maria et al., 2004; Lehmann et al., 2005).

Fourteen categories are used to classify all of the 595 resolved particles based on similar spectral features. Between 1 and 76 particles were analyzed on each of the 38 slides; the number of spectra categories on each slide ranged from one to nine. Fig. 1 shows the different spectra types and Fig. 2 shows the corresponding size, shape classification, and project from which each spectra was collected. Fig. 3 presents example images of

Table 1
Summary of samples analyzed by STXM

Field campaign	Study period; location	Min. Alt. (m)	Max. Alt. (m)	Number of particles
PELTI	Jul 2000; Caribbean (NCAR C-130)	30	2300	75
ACE-Asia	Apr 2001; Sea of Japan (NCAR C-130)	30	3650	185
DYCOMS II	Jul 2001; NE Pacific S. Cal. coast (NCAR C-130)	200	540	106
New Jersey	Aug 2003; Princeton, New Jersey (ground site)	85		48
MILAGRO (Urban)	Mar 2006; Mexico City (urban ground site)	2200		69
MILAGRO (Aircraft)	Mar 2006; Mexico mainland/Yucatan peninsula (NCAR C-130)	2090	4340	95
INTEX-B	May 2006; U.S. West coast (NCAR C-130)	890	1920	17
Total				595

Campaign	Spectra type													
	(a)	(b)	(c)	(d)	(e)	(f)	(g)	(h)	(i)	(j)	(k)	(l)	(m)	(n)
PELTI	14	0	0	4	5	12	0	0	14	4	23	4	0	0
DYCOMS II	41	0	25	4	2	0	0	0	14	5	16	18	10	0
ACE-Asia	46	0	0	0	0	0	0	0	2	4	17	2	0	0
New Jersey	3	0	0	3	15	0	9	0	2	2	4	10	0	0
MILAGRO (Urban)	22	0	0	4	3	0	0	9	15	10	2	5	3	8
MILAGRO (Aircraft)	9	21	0	18	8	0	2	1	6	6	7	23	1	1
INTEX-B	6	0	1	2	2	0	0	0	6	0	0	2	0	1
Total	141	21	26	35	35	12	11	10	59	31	69	64	14	10

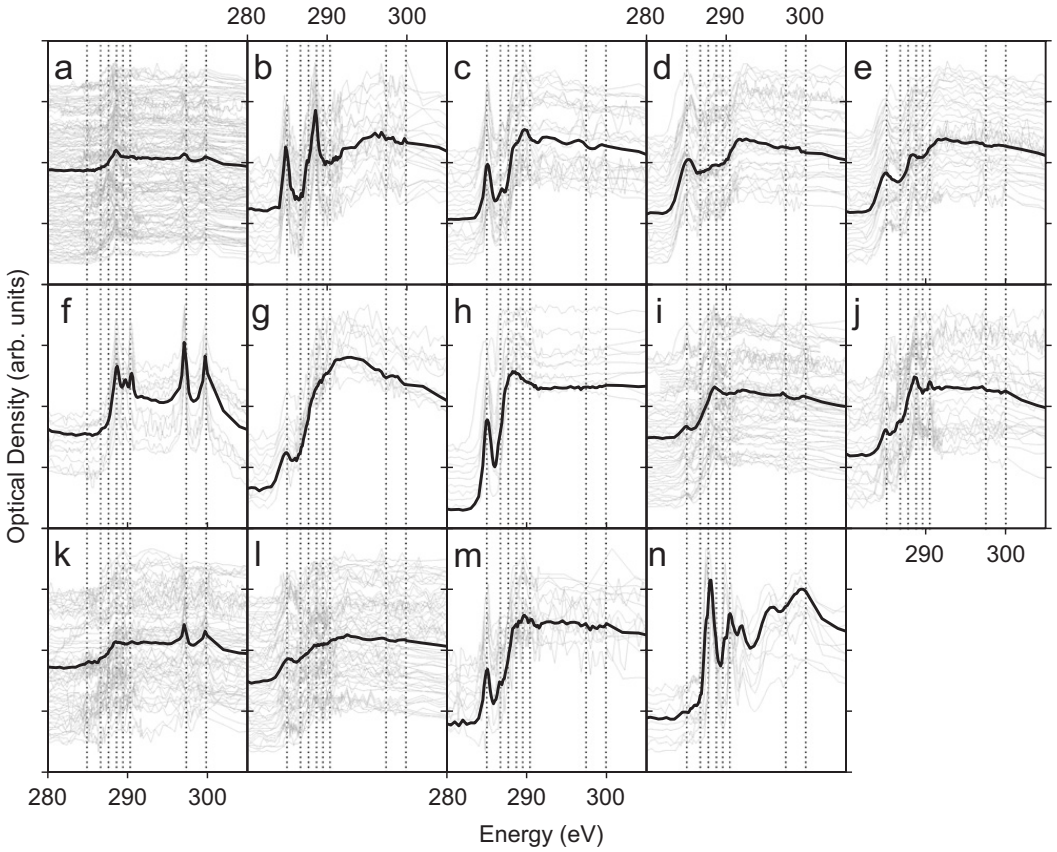

Fig. 1. Fourteen classifications of spectra. Gray lines are scaled individual spectra; dark lines are averages of all spectra. Individual spectra include arbitrary shifts on the vertical axis to display them separately. Vertical lines at 285, 286.7, 287.7, 288.7, and 290.4 eV represent R(C═C)R′, R(C═O)R, R(CH_n)R′, R(C═O)OH, and CO_3^{2-} transitions, respectively.

particles corresponding to each particle type. These images are not meant to be representative of each category, but, collectively, illustrates some of the diversity observed in morphology of ambient particles. While there is insufficient evidence to assert this set of categories is a complete representation of atmospheric organic particle types, it is surprising that a few types appear in many disparate regions of the atmosphere. Other particle types appear only in one or two specific regions, suggesting their sources may be more limited.

3.1. Spectra types and descriptions

The most ubiquitous type of spectra was that dominated by an R(C═O)OH peak (Fig. 1a), designated as type a. There were 136 particles that exhibited this spectrum. These types of particles were found at some of the samples from every project and over a wide size range, in both spherical and irregular form. A particularly high number of submicron, spherical particles of this type were found in DYCOMS II and ACE-Asia.

Type b spectra (Figs. 1b and 2b) were observed exclusively on a single sample from Research Flight 6 during the MILAGRO campaign. These spectra strongly indicated the presence of both R(C═C)R′ and R(C═O)OH bonds (Fig. 1b). All type b particles (21) were submicron and spherical (no heterogeneities were detected). Particles on this slide were collected on the afternoon of a holiday weekend (18 March 2006) northeast of Mexico City. Absorbances in R(C═C)R′ and R(C═O)OH of type b spectra are distinguished by very strong and distinct peaks.

Type c (Figs. 1c and 2c) was predominantly found in the ACE-Asia particles, and shows a peak in the R(C═O)R region in addition to R(C═O)OH and R(C═C)R′. These particles were identified as being surface-oxidized primary carbon, possibly black carbon (Maria et al., 2004). There were 25 type c spectra, only one of which was from the INTEX-B study. Type c included spherical and irregular particles. The spherical ones ranged from 0.3 to 1.4 μm in diameter ($n = 15$), and irregular ones ranged from 0.6 to 5 μm in diameter ($n = 10$).

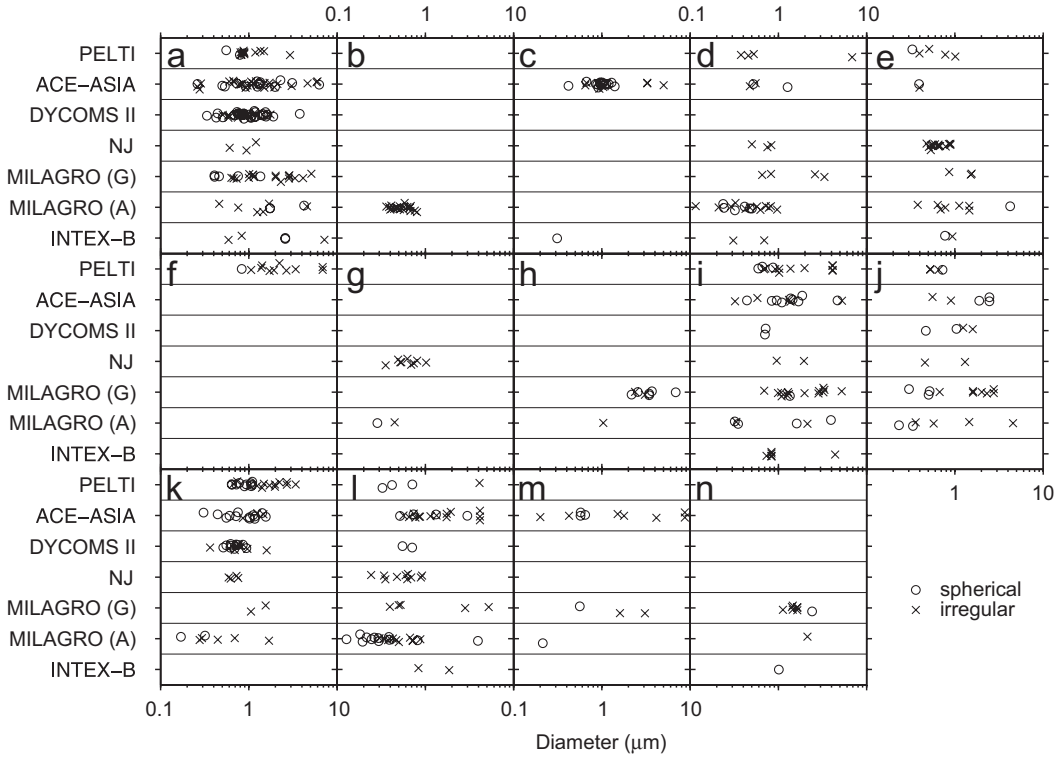

Fig. 2. Size and shape classification of particles by spectra type; each panel corresponds to the spectra shown in respective panels of Fig. 1. Circles indicate spherical particles, and crosses indicate irregular particles.

These particles were generally not associated with heterogeneities.

Type d (Figs. 1d and 2d) was observed in almost every field campaign, especially in airborne measurements. Type d spectra are dominated by a strong absorbance in the R(C═C)R′ region (Fig. 1d), without the distinct peaks observed in Fig. 1b. These particles are generally submicron and irregular, with a few exceptions. While many of the type d particles were irregular, only one of them had a detectable heterogeneity.

Fig. 1e shows type e spectra with strong absorbance around R(C–H)R′ and R(C═O)OH in addition to R(C═C)R′. These particles were collected mostly on the aircraft during MILAGRO and also in Princeton, NJ.

Type f (Figs. 1f and 2f) was found exclusively in PELTI samples, showing a strong R(C═O)OH abundance and high absorbances in the K region, consistent with either a dust or biomass burning source. Concurrent absorbance in the region of CO_3^{2-} absorbance suggests a strong mineral contribution.

Fig. 1g shows spectra of particles collected mostly in Princeton for combustion-related aerosols (Maria et al., 2004). Additional type g samples were also found in MILAGRO aircraft measurements. These show a strong absorbance in the R(C═C)R′ region and amorphous absorbance in R(C–H)R′ and R(C═O)OH just before the carbon K-edge.

Type h spectra shown in Figs. 1h and 2h were collected mostly in Mexico City with the exception of one collected on board the NCAR C-130 near Mexico City—these particles are spherical and supermicron. Because of their size, these particles are often associated with heterogeneities, in the form of inorganic inclusions or enrichment of R(C═O)OH at the surface.

Five additional spectra types include spectra with a common presence of functional groups but with varying abundances of each component (Figs. 1 and 2, i–m). Spectra in Fig. 1i show strong absorbance in regions of R(C═O)OH and R(C═C)R′. Type j spectra are similar to type c spectra (ACE-Asia particles) with R(C═C)R′, R(C═O)R, R(C═O)OH absorbance but weaker R(C═C)R′. Type k spectra show the carbon K-edge but no significant peaks. Type l shows R(C═C)R′ absorbance, although R(C═O)OH is not discernible. Type m shows absorbance in R(C═C)R′ and

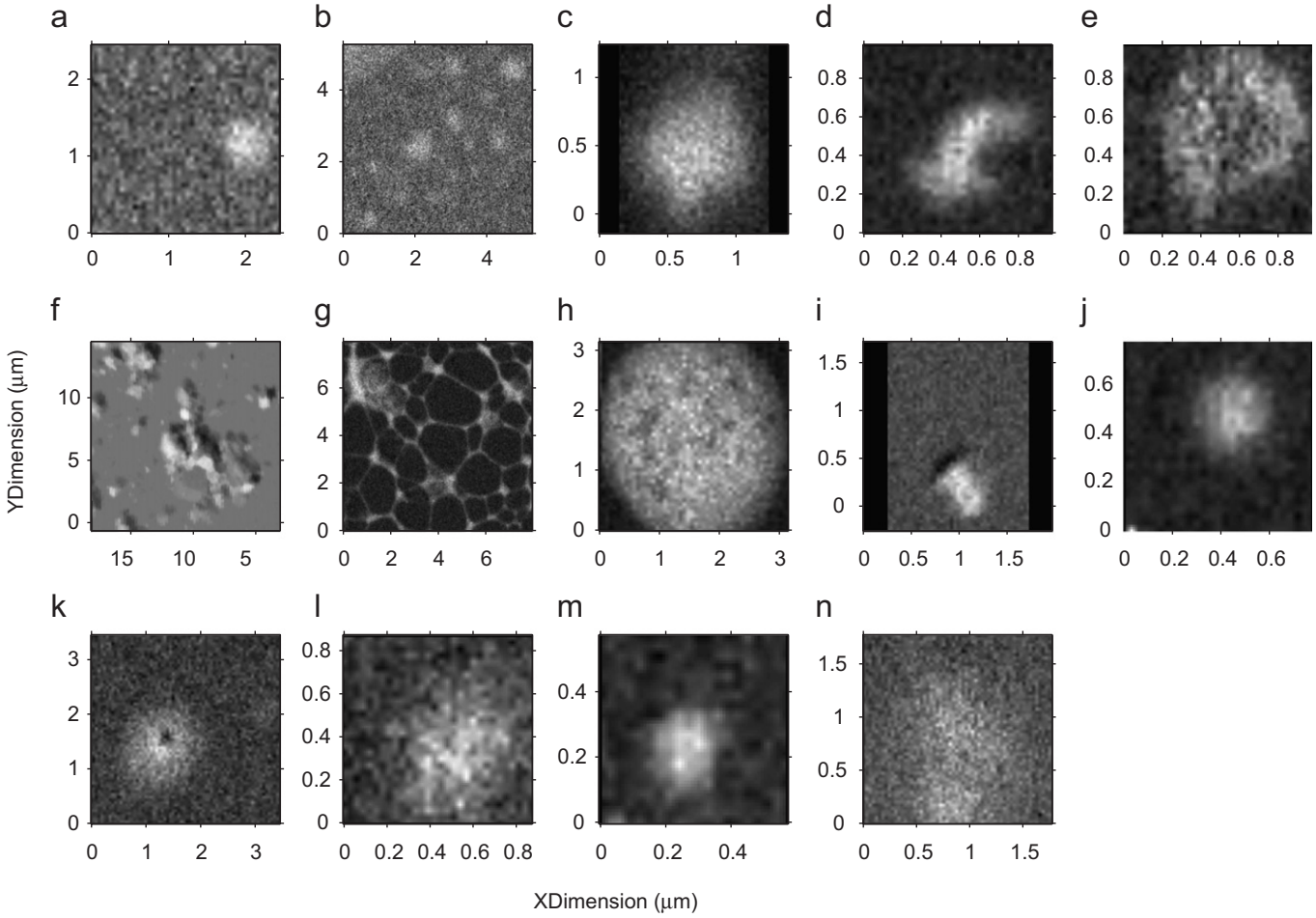

Fig. 3. Example images for each category; each panel corresponds to respective panels in Fig. 1. Particles are from (a) ACE-ASIA, (b) MILAGRO (A), (c) ACE-ASIA, (d) MILAGRO (A), (e) MILAGRO (U), (f) PELTI, (g) Princeton, (h) MILAGRO (U), (i) ACE-ASIA, (j) MILAGRO (A), (k) ACE-ASIA, (l) MILAGRO (A), (m) MILAGRO (A), (n) MILAGRO (U).

R(C═O)R, but in general R(C═O)OH absorbance is not apparent. Altogether, these five groups account for 35% of the particles.

Type n shows a maximum peak between R(C═H)R′ and R(C═O)OH absorbance regions with additional unidentified peaks (Fig. 1n). Such shifts in peak absorbance energies can occur in response to subtle differences in local coordination environment. These particles were collected mostly in Mexico City but also aloft during MILAGRO and INTEX-B, and these particles were generally found to be larger than 1 μm (Fig. 2n).

3.2. Atmospheric implications

The measured properties of organic functional groups in atmospheric particles and comparison of overall absorbance features with reference spectra suggest possible particle sources and radiative impacts. Below we consider the potential atmospheric sources of some of the mixture types we have identified, by classifying them as combustion-derived, carboxylic-acid dominated, biogenic aerosols, and unidentified.

3.2.1. Strongly aromatic aerosols

Types b–e, g, h, and m share significant absorbance in the R(C═C)R′ region (Fig. 5A) and possibly indicate the presence of sp^2-bonding of carbon found in soot or black carbon, suggesting that these particles will most likely be strongly absorbing. The degree of graphitization is dependent on fuel type and conditions of combustion (Andreae and Gelencser, 2006; Bond and Bergstrom, 2006), which Braun and coworkers have observed by NEXAFS and X-ray scattering in controlled studies (Braun, 2005; Braun et al., 2005b, 2006a, 2007; di Stasio and Braun, 2006). Hopkins et al. (2007) used an $\%sp^2$ hybridization metric to distinguish among different types of

spectra measured for reference and field samples of aerosol, and these values ranged from 29% to 82%. In our particle classes, we observed mean values ranging from 28% to 72% (Table 2). Significant differences in $\%sp^2$ within each particle class exist such that relating variations in NEXAFS spectra of ambient particles to combustion conditions is difficult, but it is sufficient to note that sp^2-hybridization in graphitic carbon is strongly related to photoabsorption and index of refraction (Bond and Bergstrom, 2006).

While "black carbon" is often used synonymously with "soot" to refer to the major light-absorbing component of aerosols, Andreae and Gelencser (2006) note that the contribution in light absorption from other carbonaceous compounds can also be significant. "Brown carbon" compounds may include other anthropogenic combustion-related compounds such as coal tar or products of organic matter (e.g., lignin) pyrolysis, but also biogenic materials such as humic or fulvic substances, humic-like substances (HULIS), products of aromatic hydroxy acid oxidation and reactions of organic compounds in sulfuric acid particles (Andreae and Gelencser, 2006).

Backtrajectories of types c and d particles were analyzed by Maria et al. (2004) and suggest their origins may lie in combustion sources. Several possible origins of type b spectra were considered, including contamination. Another compound which has a strong signature of absorbance in R(C═C)R′ and R(C═O)H is phthalic acid (Plaschke et al., 2004), commonly used as plasticizer in many plastic materials (and possibly a contributor to sampling artifact; Fraser et al., 2003; Ray and McDow, 2005). Out of the 30 particles identified on this slide, nine of the particles did not contain this chemical fingerprint, though such evidence may be produced by preferential absorption by a certain class of particle. The lack of this type of spectra in other samples, however, indicates that if it were contamination, it would be generated from an isolated event. So other explanations are more likely. For instance, phthalic acid is often found in atmospheric aerosols (e.g., Limbeck et al., 2001; Rudolph and Stupak, 2002; Ray and McDow, 2005; Kawamura and Yasui, 2005), from direct emission by combustion sources (Kawamura and Kaplan, 1987) or secondary formation by oxidation of aromatic hydrocarbons (Jang and McDow, 1997; Fraser et al., 2003; Fine et al., 2004; Wang et al., 2006). However, type b spectra may be considered only partially phthalic-acid-like, in that the proportion of the peaks are reversed. For type b particles the relative abundance of R(C═O)H is greater than that of R(C═C)R′, while the opposite is true in phthalic acid. It is also possible that type b spectra represent another class of compounds with strong sp^2-bonding combined with carboxylic acid groups.

Backtrajectories for type b particles (Fig. 4A) indicate that they traveled from the southeast of Mexico City at least 1500 m above ground level. Concurrent measurements of elemental composition by XRF indicate relatively high loadings of Barium. Barium is also used in rubber production and can be a airborne product of tire abrasion (e.g., Weckwerth, 2001; Varrica et al., 2003), but such particles are often coarse and irregularly shaped—unlike type b particles (Fig. 3b). Barium can also be found in pyrotechnic aerosols (i.e. from fireworks; Liu et al., 1997). The day on which this sample was collected was a holiday weekend in Mexico. Magnesium is often associated with Barium in pyrotechnic particles, but XRF measurements indicate negligible concentrations were present in this sample. Since the relative quantities of Barium and Magnesium in these types of aerosols can vary (Liu et al., 1997), the absence may be a result of the detection limit.

Another possible source of Barium is volcanic emissions. The backtrajectory analysis indicates the air parcel passed by the location of Popocatepetl, an active volcano that contributes to SO_2 burdens in the nearby City. It is possible that type b particles are derived from this source. The XRF analysis also indicates high loadings of Sulfur, which is in agreement with the findings by Obenholzner et al. (2003), who measured Ba–S–O particles (presumably found in the form of barite, $BaSO_4$) from this volcanic plume.

Table 2
$\%sp^2$ Hybridization

Metaclass	Type	Mean (%)	Standard deviation (%)
Strongly aromatic	b	48	5
	c	40	12
	d	72	15
	e	56	10
	g	29	8
	h	39	18
	m	28	18
Multiple transition	i	18	15
	j	30	20

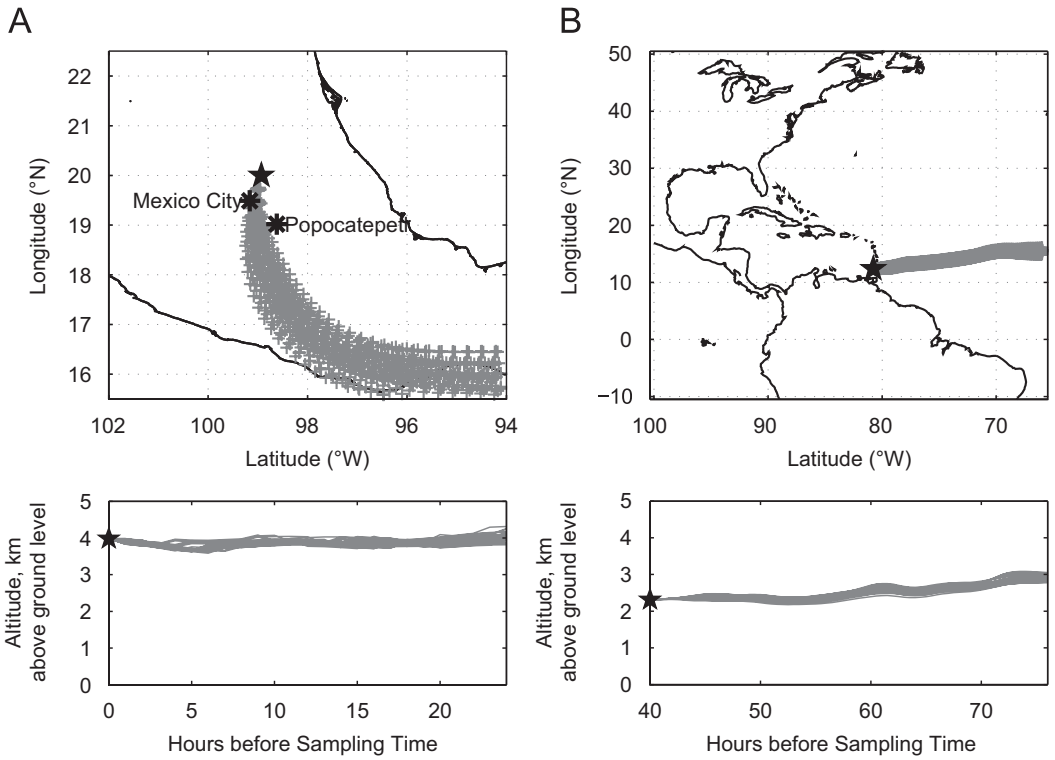

Fig. 4. Backtrajectories obtained from NOAA HYSPLIT simulations for particle types b (panel A) and f (panel B). Star symbol indicates locations from which backtrajectories were calculated. Initial conditions, panel A: 3/18/06 21:00 GMT, 20.00N, 98.93W, 3980 m above MSL, 24-h duration; panel B: 2000-07-21 15:00 GMT, 23.39N, 61.55W, 2470 m above MSL, 72-h duration.

The other types of particles in this category were prevalent over many locations and field campaigns indicating non-unique origins. However, comparisons with reference spectra of soot particles examined under various conditions (e.g., Brandes et al., 2004; Braun et al., 2004, 2005a, b; Michelsen et al., 2007; Lehmann et al., 2005; some examples shown with average spectra from 1 in Figs. 6A and B) show many similarities, including the absorption of X-rays in R(C═C)R′ and R(C═O)OH regions. Differences may arise from one of many possible reasons. For instance, soot spectra can vary depending on fuel source and engine loading (Braun et al., 2005a, b), condensed-phase hydrocarbons can be co-emitted with soot as a coating layer (Braun et al., 2004; Kis et al., 2006), and rapid internal mixing with inorganic compounds have been observed in freshly emitted soot particles in an urban environment (Johnson et al., 2005). In the absence of these mixing mechanisms, however, the hydrophobicity of soot and its low probability for removal by wet deposition (Lim et al., 2003) may account for the frequent observation of these particles, especially at high altitudes.

Mishchenko and coworkers found that the single scattering albedo calculated by Mie theory is not very sensitive to non-sphericity (Mishchenko et al., 1995), but shape considerations can still influence the radiative budget if the excess surface area of irregular particles over that of spherical particles is taken into account. Scattering is a strong function of hygroscopic growth of particles. Irregular particles of initially hydrophobic composition such as soot can become more hydrophilic with increasing surface area (van Poppel et al., 2005; Petters et al., 2006). Of our soot-like particles, 70 out of 88 are irregular. Our sample collection method may bias our results toward an irregular classification as the process of impaction can alter the shape of spherical particles. Spherical particles may indicate that these hydrophilic conversions have taken place and these soot inclusions have water associated with them (wet particles are almost always spherical, Seinfeld and Pandis, 2006). While the resolution of STXM does not permit rigorous fractal analysis, van Poppel et al. (2005) found that when the fractal properties of fresh soot aggregates are explicitly calculated with 3D images assembled from TEM and electron tomography, the surface area increased by an order of magnitude over that of a spherical particle of "equivalent" size. Taking into account only the (sulfuric acid) condensation pathway, their

simulations in a global climate model suggested that BC lifetime and direct radiative forcing are currently underestimated by 40%. The coating will further accelerate the black-carbon absorption enhancement described by Jacobson (2000).

Mishchenko et al. (2004) found that agglomerations of scattering aerosol components that retain chemically distinct phases have similar optical properties to an ensemble of externally mixed particle population composed of the same species. However, black carbon internally mixed (coated) with even purely scattering chemical components can become more absorbing and contribute significantly to climate change (Jacobson, 2000). NEXAFS spectra are sensitive to combustion conditions under which organic aerosols are formed and to subsequent atmospheric processing by ultraviolet radiation and oxidants, providing complementary information for source identification of particles (Braun, 2005; Braun et al., 2006a, 2007; di Stasio and Braun, 2006). Several authors (e.g., Posfai et al., 1999; Johnson et al., 2005) report that soot coated by inorganics is common in the atmosphere. In our data, 82 out of 88 soot-like particles contain non-zero intensities below 283 eV, showing the presence of non-carbonaceous components in the particles.

3.2.2. *Multiple-transition aerosols*

Types i and j include particles that show absorptions in R(C═C)R′ (though relatively weaker than the soot-type particles), R(C═O)R, R(C–H)R′ and R(C═O)OH (Fig. 5B); some studies identify absorbances around 286 eV as those belonging not only to ketonic carbonyl but also to C–OH resonances of hydroxylated aromatics such

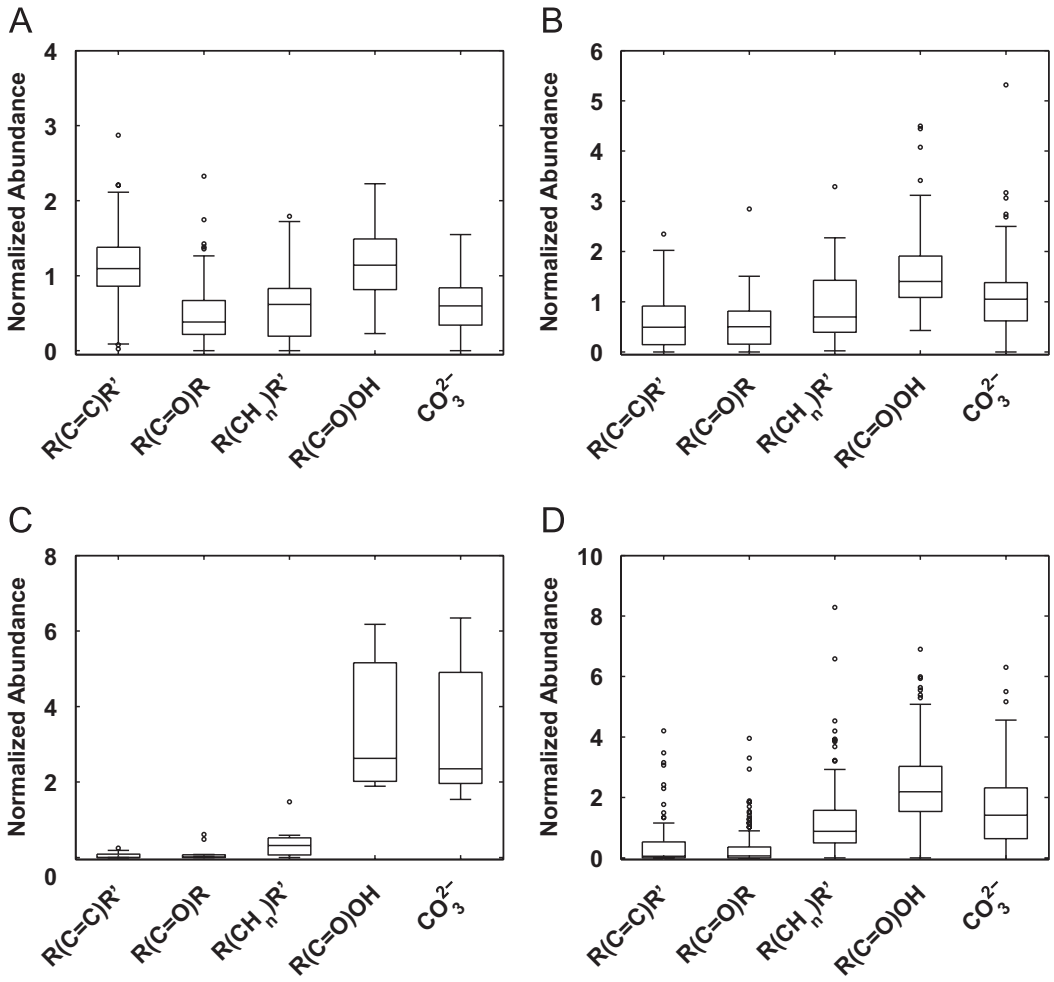

Fig. 5. Peak areas normalized by total carbon content for four metaclasses: panel A, strongly aromatic; panel B, multiple-transition; panel C, carbonate and carboxylic-carbonyl; and panel D, carboxylic-carbonyl dominated aerosols. Boxes encompass the 25th to 75th percentile of the data, lines within boxes represent the median value, and whiskers span 1.5 times the interquartile range. Circles represent data points that lie outside of this range.

as phenols (e.g., Lehmann et al., 2005; Schumacher et al., 2005; Braun, 2005), which can be significant for products of wood burning (Braun, 2005). These particle types share spectral features most similar to those found in biogenic sources: humic and fulvic acids (Ade and Urquhart, 2002), soil substances (Solomon et al., 2005; Lehmann et al., 2005; Schumacher et al., 2005), and biomass combustion (Braun, 2005; Tivanski et al., 2007). Reference spectra for some of these aerosols published in the literature are shown with average spectra of types i and j particles in Figs. 6C and D.

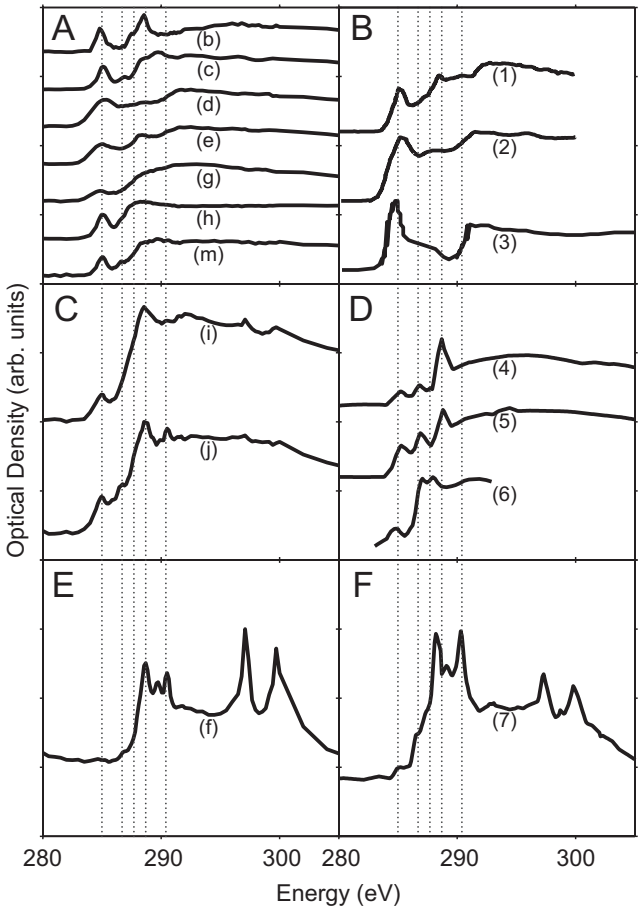

Fig. 6. NEXAFS spectra of reference material. Panels A, C, and E are spectra shown in Fig. 1. Panel A, average spectra of strongly aromatic aerosols. Panel B, combustion-derived aerosol: (1) black-carbon-like spectra of marine particulate organic matter from factor analysis (Brandes et al., 2004), (2) diesel soot (Braun, 2005), (3) graphitic carbon (di Stasio and Braun, 2006). Panel C, average spectra of multiple-transition aerosols. Panel D, (4) fulvic acid (Ade and Urquhart, 2002), (5) humic acid (Ade and Urquhart, 2002), (6) wood-smoke particles collected on a chimney (Braun, 2005). Panel E, average spectra of carbonate and carboxylic-carbonyl aerosol (type f) particles collected over the Caribbean Ocean during PELTI campaign. Panel F, (7) pine Ultisol soil (Ade and Urquhart, 2002). Vertical lines at 285, 286.7, 287.7, 288.7, and 290.4 eV represent R(C═C)R′, R(C═O)R, $R(CH_n)R'$, R(C═O)OH, and CO_3^{2-} transitions, respectively.

%sp^2 hybridization in biomass burning aerosols studied by Hopkins et al. (2007) ranged from 5% to 41%; Suwannee river humic and fulvic acids studied by the same authors were 28% and 29%, respectively, indicating generally lower values than those calculated for black-carbon aerosols. The average %sp^2 hybridization calculated for i and j particles (18% and 30%, respectively) are in qualitative agreement with this trend. For particles generated from biomass (wood) combustion, however, it is possible that the absorbance at 285 eV can be attributed to polycyclic aromatic hydrocarbons (PAHs; Rogge et al., 1998) rather than the sp^2-bonding anticipated in black carbon.

HULIS in the atmosphere have received considerable attention in the aerosol literature (e.g., Gelencser et al., 2002; Gysel et al., 2004; Hoffer et al., 2006; Graber and Rudich, 2006 and references therein). In comparison with reference spectra of humic and fulvic acids studied by Ade and Urquhart (2002), particles contained in types i and j categories may be examples of atmospheric particles identified elsewhere as HULIS. Tivanski et al. (2007) studied tarballs, a special class of aerosols generated by biomass-burning events, also by NEXAFS spectroscopy, and observed similarities in the presence of R(C═C)R′, R(C═O)R, and R(C═O)OH transitions as seen in similar reference acid standards.

HULIS in aerosols have polycyclic ring structures and hydrocarbon side chains, hydroxyl, carboxyl, and carbonyl groups (Graber and Rudich, 2006), and this is in agreement with our observation of X-ray absorbances over a wide range of energies. Despite the overall resemblance to humic and fulvic acid samples, there are a few important spectral differences. The differences may reflect the dissimilarity between atmospheric HULIS and fulvic acids and laboratory-generated macromolecules, most importantly in the small molecular size of the former type (Graber and Rudich, 2006). Graber and Rudich (2006) attribute this difference to a number of possible causes, including abiotic formation mechanisms in airborne particles, processing (i.e. photo-oxidation) in the atmosphere, and ionic interference toward the congregation of polymeric units.

If types i and j particles are indeed derived from sources of brown carbon substances described by Andreae and Gelencser (2006), they may serve as

additional light-absorbing material in the atmosphere. For instance, the water-soluble HULIS obtained from biomass burning aerosol was shown to absorb strongly at shorter wavelengths, to the sum of about 7% over the solar spectrum (Hoffer et al., 2006). Water-soluble material resembling humic substances has been observed to have low to comparable water uptake to secondary organic aerosol (SOA) and may alter the water uptake and phase-transition properties of inorganic aerosol (Gysel et al., 2004; Badger et al., 2006). Of 115 of these types of particles, 70 were spherical.

3.2.3. Carbonate and carboxylic-carbonyl aerosol

Type f particles were collected over the Caribbean Ocean during the PELTI campaign (Maria et al., 2002). As seen in Fig. 5C, these particles show high relative abundance of R(C═O)H and also CO_3^{2-}. Type f spectra strongly resemble the spectrum of pine Ultisol soil collected in Puerto Rico (Ade and Urquhart, 2002, shown in Figs. 6C and D). These particles may have either traveled from Africa with dust of similar composition as indicated by the backtrajectory analysis (Fig. 4B), or they could be produced from local sources by vertical mixing of soil dust particles.

3.2.4. Carboxylic-carbonyl dominated organic aerosol

Type a particles have a strong carboxylic carbonyl signature (Fig. 5D), and these particles are likely to behave differently from the light-absorbing carbon in the atmosphere. Carboxylic acids and oxygenated compounds are relatively soluble and can thus be significant players in direct radiative forcing and also as cloud condensation nuclei (Kanakidou et al., 2005). Myhre and Nielsen (2004) calculated that several binary mixtures of organic acids (oxalic, malonic, tartronic, succinic, and glutaric) with water have a purely scattering effect, which is less dependent on component than on mass mixing ratio in solution. Fifty-eight of 136 type a particles were spherical. For hydrophilic species to be irregular suggests that impaction resulted in an asymmetrical distortion of particle shape, or in efflorescence of the particle. Carboxylic acids are the dominant product of reactions yielding SOA (Yu et al., 1999; Glasius et al., 2000), contributing as much as 30% to the SOA mass yield of α-pinene ozonolysis (Yu et al., 1999). Their formation mechanism suggests one reason for their ubiquity in different locations and field sampling campaigns.

3.2.5. Unidentified spectra types

The remaining spectra types have not been identified with specific organic compounds or sources, in part because of the paucity of reported spectra for other potential sources of organic aerosol (e.g. isoprene, glyoxyl, SOA, condensation products of primary emissions of intermediate volatility). Furthermore, mixing of particle components and heterogeneous reactions in the atmosphere will induce chemical transformations in the aerosol phase, some or all of which will affect the measured NEXAFS spectra.

The main peak in type n is in the region of R(C═O)OH but is shifted slightly from similar peaks observed in all other samples, indicating a bonding environment different from those found in the rest of the particles. The origin and chemistry that drives this shift in absorbance energy level is unclear. Types k and l particles lack distinct spectral features; in particular, there is an absence of a carboxylic peak. The total carbon to total mass ratio calculated by the method of Maria et al. (2004) indicates that on average, the normalized carbon content of these particles are comparable to those from other particles, suggesting that the absence of these peaks is not necessarily due to the lack of carbonaceous material. Several alternative explanations are possible. Braun and coworkers have studied the effect of chemical changes to diesel particulate matter and the impact on molecular bonding observed by NEXAFS. In one study, Braun (2005) showed that diesel particulate matter "weathered" in ambient humidity and sunlight for 10 days resulted in a decrease in R(C═O)OH and C–OH resonances but an increase in R(C═C)R′. Braun et al. (2006b) observed decomposition of carboxyl groups in alginic acid and diesel soot extracts to carbonate by NEXAFS under intense X-ray irradiation. The authors of the study suggest such transformations are likely to be slow but possible in soot particles in the atmosphere. In addition, carboxylic acids can be converted into high-molecular weight organic compounds (Mochida et al., 2006), or gas-phase oxidants can increase the oxygen content in the reacted organic layer (Katrib et al., 2005) which might decrease the R(C═O)OH absorbance and increase the R(C═O)R′ absorbance. The collective effects of all aging processes on the chemical transformation

of aerosols in the atmosphere are still uncertain, and the extent that such chemical changes can be detected with NEXAFS C(1s) is not yet known.

4. Conclusions

As a first approximation, sampling an air mass with $\sim$1000 particles cm^{-3} at 1 Lpm for 20 min will result on the order of 10^7 particles. Of the ones that can be identified by STXM (>100 nm), we typically analyze between 1 and 76 particles per sample. The frequency of occurrence of certain types of spectra and morphology suggests that they may represent a significant part of the ambient particle population, even though this small sample cannot be extrapolated to all atmospheric particles.

Spectra were classified into 14 types on the basis of similarities in the presence and relative abundance of organic functional groups. Compared to classification techniques by other instruments (e.g., AMS, Zhang et al., 2005a; ETEM, Semeniuk et al., 2007), STXM provides more detailed organic classification by chemical bond characteristics for individual particles using NEXAFS. Using this information, our work suggests one scheme for representing the multitude of condensed-phase organic compounds in the atmosphere with a reasonable number of mixtures and particle types.

The observed combinations of particle shape and carbon K-edge spectra indicate that many classes of organic particles exist in the atmosphere, even within the same geographical location. A few spectra classes were unique to specific locations, but many types of carbonaceous particles with similar molecular bonding structures exist in disparate regions around the globe, suggesting common types of sources and similar processes of atmospheric transformations for organic particles. Examining similarities with reference spectra, black carbon, humic-like, pine ultisol, and secondary or processed aerosols were identified in several field campaigns in the northern hemisphere. The existence of different types of organic compounds on different organic particles may affect CCN properties, interaction with solar radiation, and aerosol chemistry differently.

Acknowledgments

The authors acknowledge grant support for this work from DOE (W/GEC05-010, MPC35TA-A5), NSF (ATM-0511772, ATM-0408501, ATM-0002035, ATM-0104707), and the James S. McDonnell Foundation. In addition, valuable assistance was provided in using and interpreting ALS facilities by S.C.B Myneni and M.K. Gilles. J.R. Anderson, M.D. Rivera, R. Ramos, and the science and operation teams of the field experiments PELTI, ACE-Asia, DYCOMS II, MILAGRO, and INTEX-B also provided enormous assistance in sample collection. The authors also thank the anonymous reviewers for their insight and helpful comments.

References

Ade, H., Urquhart, S.G., 2002. NEXAFS spectroscopy and microscopy of natural and synthetic polymers. Chemical Applications of Synchrotron Radiation. World Scientific Publishing, Singapore.

Andreae, M.O., Gelencser, A., 2006. Black carbon or brown carbon? The nature of light-absorbing carbonaceous aerosols. Atmospheric Chemistry and Physics 6, 3131–3148.

Badger, C.L., George, I., Griffiths, P.T., Braban, C.F., Cox, R.A., Abbatt, J.P.D., 2006. Phase transitions and hygroscopic growth of aerosol particles containing humic acid and mixtures of humic acid and ammonium sulphate. Atmospheric Chemistry and Physics 6, 755–768.

Barkay, Z., Teller, A., Ganor, E., Levin, Z., Shapira, Y., 2005. Atomic force and scanning electron microscopy of atmospheric particles. Microscopy Research and Technique 68 (2), 107–114.

Bein, K.J., Zhao, Y.J., Wexler, A.S., Johnston, M.V., 2005. Speciation of size-resolved individual ultrafine particles in Pittsburgh, Pennsylvania. Journal of Geophysical Research—Atmospheres 110 (D7).

Bond, T.C., Bergstrom, R.W., 2006. Light absorption by carbonaceous particles: an investigative review. Aerosol Science and Technology 40 (1), 27–67.

Brandes, J.A., Lee, C., Wakeham, S., Peterson, M., Jacobsen, C., Wirick, S., Cody, G., 2004. Examining marine particulate organic matter at sub-micron scales using scanning transmission X-ray microscopy and carbon X-ray absorption near edge structure spectroscopy. Marine Chemistry 92 (1–4), 107–121.

Braun, A., 2005. Carbon speciation in airborne particulate matter with C (1s) NEXAFS spectroscopy. Journal of Environmental Monitoring 7 (11), 1059–1065.

Braun, A., Shah, N., Huggins, F.E., Huffman, G.P., Wirick, S., Jacobsen, C., Kelly, K., Sarofim, A.F., 2004. A study of diesel PM with X-ray microspectroscopy. Fuel 83 (7–8), 997–1000.

Braun, A., Huggins, F.E., Shah, N., Chen, Y., Wirick, S., Mun, S.B., Jacobsen, C., Huffman, G.P., 2005a. Advantages of soft X-ray absorption over TEM-EELS for solid carbon studies—a comparative study on diesel soot with EELS and NEXAFS. Carbon 43 (1), 117–124.

Braun, A., Shah, N., Huggins, F.E., Kelly, K.E., Sarofim, A., Jacobsen, C., Wirick, S., Francis, H., Ilavsky, J., Thomas, G.E., Huffman, G.P., 2005b. X-ray scattering and spectroscopy studies on diesel soot from oxygenated fuel under various engine load conditions. Carbon 43 (12), 2588–2599.

Braun, A., Huggins, F.E., Kelly, K.E., Mun, B.S., Ehrlich, S.N., Huffman, G.P., 2006a. Impact of ferrocene on the structure of diesel exhaust soot as probed with wide-angle X-ray scattering and C(1s) NEXAFS spectroscopy. Carbon 44 (14), 2904–2911.

Braun, A., Wirick, A., Kubatova, A., Mun, B.S., Huggins, F.E., 2006b. Photochemically induced decarboxylation in diesel soot extracts. Atmospheric Environment 40 (30), 5837–5844.

Braun, A., Mun, B.S., Huggins, F.E., Huffman, G.P., 2007. Carbon speciation of diesel exhaust and urban particulate matter NIST standard reference materials with C(1s) NEXAFS spectroscopy. Environmental Science & Technology 41 (1), 173–178.

di Stasio, S., Braun, A., 2006. Comparative NEXAFS study on soot obtained from an ethylene/air flame, a diesel engine, and graphite. Energy Fuels 20 (1), 187–194.

Draxler, R.R., Rolph, G.D., 2003. Hysplit (hybrid single-particle lagrangian integrated trajectory). Model access via NOAA ARL READY Website (http://www.arl.noaa.gov/ready/hysplit4.html). NOAA Air Resources Laboratory, Silver Spring, MD.

Fine, P.M., Chakrabarti, B., Krudysz, M., Schauer, J.J., Sioutas, C., 2004. Diurnal variations of individual organic compound constituents of ultrafine and accumulation mode particulate matter in the Los Angeles basin. Environmental Science & Technology 38 (5), 1296–1304.

Fraser, M.P., Cass, G.R., Simoneit, B.R.T., 2003. Air quality model evaluation data for organics. 6. C-3–C-24 organic acids. Environmental Science & Technology 37 (3), 446–453.

Fuzzi, S., Andreae, M.O., Huebert, B.J., Kulmala, M., Bond, T.C., Boy, M., Doherty, S.J., Guenther, A., Kanakidou, M., Kawamura, K., Kerminen, V.M., Lohmann, U., Russell, L.M., Poschl, U., 2006. Critical assessment of the current state of scientific knowledge, terminology, and research needs concerning the role of organic aerosols in the atmosphere, climate, and global change. Atmospheric Chemistry and Physics 6, 2017–2038.

Gebhart, K.A., Schichtel, B.A., Barna, M.G., 2005. Directional biases in back trajectories caused by model and input data. Journal of Air & Waste Management Association 55 (11), 1649–1662.

Gelencser, A., Hoffer, A., Krivacsy, Z., Kiss, G., Molnar, A., Meszaros, E., 2002. On the possible origin of humic matter in fine continental aerosol. Journal of Geophysical Research—Atmospheres 107 (D12).

Glasius, M., Lahaniati, M., Calogirou, A., Bella, D.D., Jensen, N.R., Hjorth, J., Kotzias, D., Larsen, B.R., 2000. Carboxylic acids in secondary aerosols from oxidation of cyclic monoterpenes by ozone. Environmental Science & Technology 34 (6), 1001–1010.

Graber, E.R., Rudich, Y., 2006. Atmospheric HULIS: how humic-like are they? A comprehensive and critical review. Atmospheric Chemistry and Physics 6, 729–753.

Gysel, M., Weingartner, E., Nyeki, S., Paulsen, D., Baltensperger, U., Galambos, I., Kiss, G., 2004. Hygroscopic properties of water-soluble matter and humic-like organics in atmospheric fine aerosol. Atmospheric Chemistry and Physics 4, 35–50.

Hamilton, J.F., Webb, P.J., Lewis, A.C., Hopkins, J.R., Smith, S., Davy, P., 2004. Partially oxidised organic components in urban aerosol using GCXGC-TOF/MS. Atmospheric Chemistry and Physics 4, 1279–1290.

Hand, J.L., Malm, W.C., Laskin, A., Day, D., Lee, T., Wang, C., Carrico, C., Carrillo, J., Cowin, J.P., Collett, J., Iedema, M.J., 2005. Optical, physical, and chemical properties of tar balls observed during the Yosemite aerosol characterization study. Journal of Geophysical Research—Atmospheres 110 (D21).

Hoffer, A., Gelencser, A., Guyon, P., Kiss, G., Schmid, O., Frank, G.P., Artaxo, P., Andreae, M.O., 2006. Optical properties of humic-like substances (HULIS) in biomass-burning aerosols. Atmospheric Chemistry and Physics 6, 3563–3570.

Hopkins, R.J., Tivanski, A.V., Marten, B.D., Gilles, M.K., 2007. Chemical bonding and structure of black carbon reference materials and individual carbonaceous atmospheric aerosols. Journal of Aerosol Science 38, 573–591.

Huebert, B.J., Bates, T., Russell, P.B., Shi, G.Y., Kim, Y.J., Kawamura, K., Carmichael, G., Nakajima, T., 2003. An overview of ACE-Asia: strategies for quantifying the relationships between Asian aerosols and their climatic impacts. Journal of Geophysical Research—Atmospheres 108 (D23).

Huebert, B.J., Howell, S.G., Covert, D., Bertram, T., Clarke, A., Anderson, J.R., Lafleur, B.G., Seebaugh, W.R., Wilson, J.C., Gesler, D., Blomquist, B., Fox, J., 2004. Pelti: measuring the passing efficiency of an airborne low turbulence aerosol inlet. Aerosol Science and Technology 38 (8), 803–826.

Jacobson, M.Z., 2000. A physically-based treatment of elemental carbon optics: implications for global direct forcing of aerosols. Geophysical Research Letters 27 (2), 217–220.

Jang, M., McDow, S.R., 1997. Products of benz[a]anthracene photodegradation in the presence of known organic constituents of atmospheric aerosols. Environmental Science & Technology 31 (4), 1046–1053.

Johnson, K.S., Zuberi, B., Molina, L.T., Molina, M.J., Iedema, M.J., Cowin, J.P., Gaspar, D.J., Wang, C., Laskin, A., 2005. Processing of soot in an urban environment: case study from the Mexico City Metropolitan area. Atmospheric Chemistry and Physics 5, 3033–3043.

Kanakidou, M., Seinfeld, J.H., Pandis, S.N., Barnes, I., Dentener, F.J., Facchini, M.C., Dingenen, R.V., Ervens, B., Nenes, A., Nielsen, C.J., Swietlicki, E., Putaud, J.P., Balkanski, Y., Fuzzi, S., Horth, J., Moortgat, G.K., Winterhalter, R., Myhre, C.E.L., Tsigaridis, K., Vignati, E., Stephanou, E.G., Wilson, J., 2005. Organic aerosol and global climate modelling: a review. Atmospheric Chemistry and Physics 5, 1053–1123.

Katrib, Y., Martin, S.T., Rudich, Y., Davidovits, P., Jayne, J.T., Worsnop, D.R., 2005. Density changes of aerosol particles as a result of chemical reaction. Atmospheric Chemistry and Physics 5, 275–291.

Kawamura, K., Kaplan, I.R., 1987. Motor exhaust emissions as a primary source for dicarboxylic-acids in Los-Angeles ambient air. Environmental Science & Technology 21 (1), 105–110.

Kawamura, K., Yasui, O., 2005. Diurnal changes in the distribution of dicarboxylic acids, ketocarboxylic acids and dicarbonyls in the urban Tokyo atmosphere. Atmospheric Environment 39 (10), 1945–1960.

Kis, V.K., Posfai, M., Labar, J.L., 2006. Nanostructure of atmospheric soot particles. Atmospheric Environment 40 (29), 5533–5542.

Kondo, Y., Miyazaki, Y., Takegawa, N., Miyakawa, T., Weber, R.J., Jimenez, J.L., Zhang, Q., Worsnop, D.R., 2007. Oxygenated and water-soluble organic aerosols in Tokyo. Journal of Geophysical Research—Atmospheres 112 (D1).

Laskin, A., Wietsma, T.W., Krueger, B.J., Grassian, V.H., 2005. Heterogeneous chemistry of individual mineral dust particles with nitric acid: a combined CCSEM/EDX, ESEM, and ICP-MS study. Journal of Geophysical Research—Atmospheres 110 (D10).

Laskin, A., Cowin, J.P., Iedema, M.J., 2006. Analysis of individual environmental particles using modern methods of electron microscopy and X-ray microanalysis. Journal of Electron Spectroscopy and Related Phenomena 150 (2–3), 260–274.

Lehmann, J., Liang, B.Q., Solomon, D., Lerotic, M., Luizao, F., Kinyangi, J., Schafer, T., Wirick, S., Jacobsen, C., 2005. Near-edge X-ray absorption fine structure (NEXAFS) spectroscopy for mapping nano-scale distribution of organic carbon forms in soil: application to black carbon particles. Global Biogeochemical Cycles 19 (1).

Lim, H.J., Turpin, B.J., 2002. Origins of primary and secondary organic aerosol in Atlanta: results' of time-resolved measurements during the Atlanta supersite experiment. Environmental Science & Technology 36 (21), 4489–4496.

Lim, H.J., Turpin, B.J., Russell, L.M., Bates, T.S., 2003. Organic and elemental carbon measurements during ACE-Asia suggest a longer atmospheric lifetime for elemental carbon. Environmental Science & Technology 37 (14), 3055–3061.

Limbeck, A., Puxbaum, H., Otter, L., Scholes, M.C., 2001. Semivolatile behavior of dicarboxylic acids and other polar organic species at a rural background site (Nylsvley, rsa). Atmospheric Environment 35 (10), 1853–1862.

Liu, D.Y., Rutherford, D., Kinsey, M., Prather, K.A., 1997. Real-time monitoring of pyrotechnically derived aerosol particles in the troposphere. Analytical Chemistry 69 (10), 1808–1814.

Maria, S.F., Russell, L.M., Turpin, B.J., Porcja, R.J., 2002. FTIR measurements of functional groups and organic mass in aerosol samples over the Caribbean. Atmospheric Environment 36 (33), 5185–5196.

Maria, S.F., Russell, L.M., Turpin, B.J., Porcja, R.J., Campos, T.L., Weber, R.J., Huebert, B.J., 2003. Source signatures of carbon monoxide and organic functional groups in Asian Pacific Regional Aerosol Characterization Experiment (ACE-Asia) submicron aerosol types. Journal of Geophysical Research—Atmospheres 108 (D23).

Maria, S.F., Russell, L.M., Gilles, M.K., Myneni, S.C.B., 2004. Organic aerosol growth mechanisms and their climate-forcing implications. Science 306 (5703), 1921–1924.

Michelsen, H.A., Tivanski, A.V., Gilles, M.K., van Poppel, L.H., Dansson, M.A., Buseck, P.R., 2007. Particle formation from pulsed laser irradiation of soot aggregates studied with a scanning mobility particle sizer, a transmission electron microscope, and a scanning transmission x-ray microscope. Applied Optics 46 (6), 959–977.

Mishchenko, M.I., Lacis, A.A., Carlson, B.E., Travis, L.D., 1995. Nonsphericity of dust-like tropospheric aerosols—implications for aerosol remote-sensing and climate modeling. Geophysical Research Letters 22 (9), 1077–1080.

Mishchenko, M.I., Liu, L., Travis, L.D., Lacis, A.A., 2004. Scattering and radiative properties of semi-external versus external mixtures of different aerosol types. Journal of Quantitative Spectroscopy & Radiative Transfer 88 (1–3), 139–147.

Mochida, M., Katrib, Y., Jayne, J.T., Worsnop, D.R., Martin, S.T., 2006. The relative importance of competing pathways for the formation of high-molecular-weight peroxides in the ozonolysis of organic aerosol particles. Atmospheric Chemistry and Physics 6, 4851–4866.

Myhre, C.E.L., Nielsen, C.J., 2004. Optical properties in the UV and visible spectral region of organic acids relevant to tropospheric aerosols. Atmospheric Chemistry and Physics 4, 1759–1769.

Myneni, S.C.B., 2002. Soft X-ray spectroscopy and spectromicroscopy studies of organic molecules in the environment. Reviews in Mineralogy & Geochemistry 49, 485–579.

Obenholzner, J., Poelt, P., Schroettner, H., Delgado, H., 2003. Particles from the plume of Popocatépetl Volcano, Volcanic Degassing. Geological Society of London, Mexico—the FESEM/EDS Approach.

Petters, M.D., Prenni, A.J., Kreidenweis, S.M., DeMott, P.J., Matsunaga, A., Lim, Y.B., Ziemann, P.J., 2006. Chemical aging and the hydrophobic-to-hydrophilic conversion of carbonaceous aerosol. Geophysical Research Letters 33 (24).

Phares, D.J., Rhoads, K.P., Johnston, M.V., Wexler, A.S., 2003. Size-resolved ultrafine particle composition analysis—2. Houston. Journal of Geophysical Research Atmospheres 108 (D7).

Plaschke, M., Rothe, J., Denecke, M.A., Fanghanel, T., 2004. Soft X-ray spectromicroscopy of humic acid europium(III) complexation by comparison to model substances. Journal of Electron Spectroscopy & Related Phenomena 135 (1), 53–62.

Posfai, M., Anderson, J.R., Buseck, P.R., Sievering, H., 1999. Soot and sulfate aerosol particles in the remote marine troposphere. Journal of Geophysical Research—Atmospheres 104 (D17), 21685–21693.

Ray, J., McDow, S.R., 2005. Dicarboxylic acid concentration trends and sampling artifacts. Atmospheric Environment 39 (40), 7906–7919.

Rhoads, K.P., Phares, D.J., Wexler, A.S., Johnston, M.V., 2003. Size-resolved ultrafine particle composition analysis, 1. Atlanta. Journal of Geophysical Research—Atmospheres 108 (D7).

Rogge, W.F., Hildemann, L.M., Mazurek, M.A., Cass, G.R., Simoneit, B.R.T., 1998. Sources of fine organic aerosol. 9. Pine, oak and synthetic log combustion in residential fireplaces. Environmental Science & Technology 32 (1), 13–22.

Rolph, G.D., 2003. Real-time environmental applications and display system (ready). Website 〈http://www.arl.noaa.gov/ready/hysplit4.html〉. NOAA Air Resources Laboratory, Silver Spring, MD.

Rudolph, J., Stupak, J., 2002. Determination of aromatic acids and nitrophenols in atmospheric aerosols by capillary electrophoresis. Journal of Chromatographic Science 40 (4), 207–213.

Russell, L.M., Maria, S.F., Myneni, S.C.B., 2002. Mapping organic coatings on atmospheric particles. Geophysical Research Letters 29 (16).

Schumacher, M., Christl, I., Scheinost, A.C., Jacobsen, C., Kretzschmar, R., 2005. Chemical heterogeneity of organic soil colloids investigated by scanning transmission X-ray microscopy and C-1s NEXAFS microspectroscopy. Environmental Science & Technology 39 (23), 9094–9100.

Seinfeld, J.H., Pandis, S.N., 2006. Atmospheric Chemistry and Physics, second ed. Wiley, New York.

Semeniuk, T.A., Wise, M.E., Martin, S.T., Russell, L.M., Buseck, P.R., 2007. Hygroscopic behavior of aerosol particles

from biomass fires using environmental transmission electron microscopy, Journal of Atmospheric Chemistry 56, 10.1007/s10874-006-9055-5.

Solomon, D., Lehmann, J., Kinyangi, J., Liang, B.Q., Schafer, T., 2005. Carbon K-edge NEXAFS and FTIR-ATR spectroscopic investigation of organic carbon speciation in soils. Soil Science Society of America Journal 69 (1), 107–119.

Stevens, B., Lenschow, D.H., Vali, G., Gerber, H., Bandy, A., Blomquist, B., Brenguier, J.L., Bretherton, C.S., Burnet, F., Campos, T., Chai, S., Faloona, I., Friesen, D., Haimov, S., Laursen, K., Lilly, D.K., Loehrer, S.M., Malinowski, S.P., Morley, B., Petters, M.D., Rogers, D.C., Russell, L., Savic-Jovac, V., Snider, J.R., Straub, D., Szumowski, M.J., Takagi, H., Thornton, D.C., Tschudi, M., Twohy, C., Wetzel, M., van Zanten, M.C., 2003. Dynamics and chemistry of marine stratocumulus—DYCOMS-II. Bulletin of the American Meteorological Society 84 (5), 579–593.

Stöhr, J., 1992. NEXAFS Spectroscopy. Springer, Berlin.

Tivanski, A.V., Hopkins, R.J., Tyliszczak, T., Gilles, M.K., 2007. Oxygenated interface on biomass burn tar balls determined by single particle scanning transmission X-ray microscopy. Journal of Physical Chemistry A 111, 5448–5458.

Tolocka, M.P., Lake, D.A., Johnston, M.V., Wexler, A.S., 2005. Size-resolved fine and ultrafine particle composition in Baltimore, Maryland. Journal of Geophysical Research—Atmospheres 110 (D7).

van Poppel, L.H., Friedrich, H., Spinsby, J., Chung, S.H., Seinfeld, J.H., Buseck, P.R., 2005. Electron tomography of nanoparticle clusters: implications for atmospheric lifetimes and radiative forcing of soot. Geophysical Research Letters 32 (24).

Varrica, D., Dongarra, G., Sabatino, G., Monna, F., 2003. Inorganic geochemistry of roadway dust from the metropolitan area of Palermo, Italy. Environmental Geology 44 (2), 222–230.

Wang, H.B., Kawamura, K., Ho, K.F., Lee, S.C., 2006. Low molecular weight dicarboxylic acids, ketoacids, and dicarbonyls in the fine particles from a roadway tunnel: possible secondary production from the precursors. Environmental Science & Technology 40 (20), 6255–6260.

Warwick, T., Ade, H., Hitchcock, H., Padmore, H., Rightor, E., Tonner, B., 1997. Soft X-ray spectromicroscopy development for materials science at the advanced light source. Journal of Electron Spectroscopy and Related Phenomena 84 (14), 85–98.

Weckwerth, G., 2001. Verification of traffic emitted aerosol components in the ambient air of Cologne (Germany). Atmospheric Environment 35 (32), 5525–5536.

Yoon, T.H., Benzerara, K., Ahn, S., Luthy, R.G., Tyliszczak, T., Brown, G.E., 2006. Nanometer-scale chemical heterogeneities of black carbon materials and their impacts on PCB sorption properties: soft X-ray spectromicroscopy study. Environmental Science & Technology 40 (19), 5923–5929.

Yu, J.Z., Cocker, D.R., Griffin, R.J., Flagan, R.C., Seinfeld, J.H., 1999. Gas-phase ozone oxidation of monoterpenes: gaseous and particulate products. Journal of Atmospheric Chemistry 34 (2), 207–258.

Zhang, Q., Alfarra, M.R., Worsnop, D.R., Allan, J.D., Coe, H., Canagaratna, M.R., Jimenez, J.L., 2005a. Deconvolution and quantification of hydrocarbon-like and oxygenated organic aerosols based on aerosol mass spectrometry. Environmental Science & Technology 39 (13), 4938–4952.

Zhang, Q., Worsnop, D.R., Canagaratna, M.R., Jimenez, J.L., 2005b. Hydrocarbon-like and oxygenated organic aerosols in Pittsburgh: insights into sources and processes of organic aerosols. Atmospheric Chemistry and Physics 5, 3289–3311.